Giant, 17, 2024, 100246

Full-length article

Small-angle neutron scattering from cellulose solutions in phosphoric acid at different water content

Gilad Alfassi[a], **Aurel Radulescu**[b], **Sapir Lifshiz-Simon**[c], **Sapir Rappoport**[c], **Yachin Cohen**[c,*]

[a] Department of Biotechnology Engineering, Braude College of Engineering, Karmiel 2161002, Israel
[b] Forschungszentrum Jülich GmbH, Jülich Centre for Neutron Science (JCNS-4) at Heinz Maier-Leibnitz Zentrum (MLZ), Garching D-85747, Germany
[c] Department of Chemical Engineering, Technion - Israel Institute of Technology, Haifa 3200003, Israel

Keywords: Cellulose dissolution, Phosphoric acid, Water content, Neutron scattering

Cellulose from biomass is an abundant and renewable alternative source for chemicals and fuels, yet its utilization by chemical or biological process requires pre-treatment in order to release the macromolecules from their tightly packed crystal structure. Phosphoric acid (PA) has been known for many years to be an efficient solvent for crystalline cellulose. It is also established that a certain quantity of water content in PA is required for efficient pretreatment. This study uses small-angle neutron scattering (SANS) measurements to evaluate cellulose dissolution in deuterated phosphoric acid (dPA), at different wt% dPA between 78 and 97 % (different D_2O content). The SANS method is useful for this purpose due to the availability of deuterated dPA, its contrast in scattering length density towards cellulose, and its low incoherent scattering cross-section. The results indicate that most of the cellulose in 2 wt% solution is dissolved in PA as individual chains, at acid content of 81–94 wt% PA. Structural differences of the dissolved cellulose in PA of the various water compositions in this range are insignificant. At 78 % dPA the cellulose crystal still seem to be disrupted, yet the structure can be modeled as mass-surface fractals of small fibrils with irregular surface, possibly due to dissolved chain segments, which are aggregated as mass fractals of rods. At 97 % dPA evidence for a small content of undissolved fibrils is noted.

Introduction

In worldwide effort to overcome depleting fossil-based energy sources and to mitigate the negative impact of climate change due to increasing greenhouse gas emission, biomass energy is considered to have a potentially significant role as an abundant and sustainable resource [1]. Cellulose, the main component of biomass, is the most abundant organic polymer, which shows enormous potential in replacing non-biodegradable materials, in addition to being a resource for chemicals and fuel [2]. Biorefineries are facilities in which biomass valorization can be carried out by a cascade of chemical and/or biochemical reactions to useful chemicals and fuels. These may play an important role in carbon–neutral energy sources if some significant techno-economic challenges are overcome, for which significant current effort is implemented [3].

* Corresponding author.
E-mail address: yachinc@technion.ac.il (Y. Cohen).
Received 29 August 2023; Received in revised form 10 December 2023; Accepted 5 February 2024

https://doi.org/10.1016/j.giant.2024.100246

Lignocellulosic biomass is by its evolutionary function recalcitrant towards biological degradation or dissolution by water or common organic solvents. It has a compact rigid structure made of cellulose microfibrils coated by hemicellulose chains within a matrix of lignin. Cellulose is composed of repeating β-d-glucopyranose molecules with $\beta-1,4$-glucan linkage forming a linear-chain polymer with three hydroxyl groups per anhydroglucose unit (AGU) [2]. Strong intra- and inter-molecular hydrogen bonds as well as stacking of rings of adjacent polymers within the cellulose crystal result in resistance to dissolution in water and many other solvents [4–7], thus hindering cellulose processing and enzymatic hydrolysis [8].

This manuscript has two parts. The first is a review of recent studies on cellulose dissolution, focusing on structural aspects: whether cellulose chains can be dissolved as individual chains, the structure of soluble supra-molecular assemblies, if present, and the role of solvent-polymer interactions. Special attention is paid to application of small-angle x-ray and neutron scattering measurements (SAXS, SANS, respectively) as crucial techniques to assess structural features of cellulose solutions. Specific attention is devoted to cellulose dissolution in aqueous phosphoric acid (PA), which has been studied for over eighty years and is used in several technologies, such as fiber spinning and treatment for enzymatic saccharification. Despite many years of research, the water content in PA suitable for dissolution, and its effect on the structure of dissolved cellulose, are still open questions. Thus, the second part of this manuscript reports on measurement and analysis of SANS from cellulose dissolved in aqueous PA, to shed light on the effect of water content on the structure of the dissolved cellulose chains.

Over the years there have been extensive studies ensued on solvents for cellulose, recently focusing on less hazardous "green" solvents [9–11]. A variety of ionic liquids (IL) were shown to be potent solvents, especially of the imidazolium family, [12–17] and their solvation mechanism is quite well understood [18]. Ammonium-based IL solutions can also be effective in dissolving cellulose, such as tetrabutylammonium chloride [19] or acetate in dimethyl sulfoxide [20–22], or aqueous tetrabutylammonium hydroxide [23–26]. It is also known for long that cellulose dissolves in aqueous NaOH solutions in a narrow range of concentrations at low temperatures [27–30], and that adding urea or thiorea enhances the solubility at these conditions [31–34]. Indeed, cellulose pretreatment by dissolution and regeneration by coagulation with water enhances the rate and conversion of enzymatic hydrolysis [35–40], by disrupting the native cellulose crystals [41] and formation of a more open network structure [42].

Cellulose has long been known to be soluble in phosphoric acid (PA), recalling a Celanese patent from 1927 [43]. Already in 1938 it was stated that complete cellulose dissolution in concentrated PA requires the presence of some water [44]. This has been related to formation of an oxonium compound of PA molecule with two water molecules per AGU [45]. PA treatment of air-dried cellulose is also a well-known method to prepare the so-called "phosphoric acid swollen cellulose (PASC)", which exhibits high reactivity for enzymatic hydrolysis by cellulase activity [46]. The facile and rapid cellulose enzymatic depolymerization has been related to restructuring of the crystalline cellulose hydrogen bond network by the PA treatment [47]. Formation of liquid crystalline solutions by dissolving cellulose in anhydrous phosphoric acid was reported [48], and cellulose yarns were fabricated from such anisotropic solutions [49]. Cellulose regenerated from PA solution can also form a stabilizing coating for oil-in-water emulsions [50]. It should be noted that aqueous PA degrades cellulose by hydrolysis, but it is long known that the rate is rather slow [44], allowing for experimental measurements and processing.

The water content of phosphoric acid is known to be critical for cellulose amorphization and dissolution. The early studies mentioned above indicated the range of 85–100 wt% PA [44]. More recent experimental data suggest that total amorphization of hydrated cellulose can be achieved using aqueous phosphoric acid solutions containing a minimum of 79–80 wt% PA [51,52]. The structural changes of microcrystalline cellulose (MCC) effected by PA treatment were monitored with the aim to attain high-quality fermentable saccharides. MCC was directly dissolved in 83 wt% PA for 10 h at 30, 50 and 70 °C [53]. Cellulose treatment with phosphoric acid, followed by regeneration, was shown to be an effective process for fabrication of cellulose hydrogel exhibiting a low crystallinity amorphous structure, as well as stable oil-in-water emulsions, stabilized by a combination of network and Pickering mechanisms. The treatment conditions selected for scale-up used MCC/water/85 wt% PA in a ratio of 1:3:50 (wt/vol/vol), at 5 °C and 24 h [50]. Cold PA at the same MCC/water/85 wt% PA was used to dissolve cellulose for conversion into nanostructures by regeneration with water. For example, treatment at 5 °C for 3 h yielded nanofibers exhibiting only non-crystalline diffraction with minimal reduction of the polymerization degree [54]. Regenerated amorphous cellulose (RAC) exhibiting enhanced enzymatic hydrolysis was easily fabricated by a series of steps, including dissolution in ice-cold PA (83.2 wt%) and regeneration in water [55]. More open fractal structure of RAC was reported by using 85 wt% PA for dissolution and organic solvents, especially 40 vol% aqueous ethanol, as the regenerating medium [56]. Highly porous and light-weight cellulose-based cryogels were prepared using 85 wt% PA, dissolving cellulose at concentrations of 0.5–8.4 wt% at 20 °C. No phosphoric acid esters of cellulose were detected in the cryogels by FTIR spectroscopy [57]. PA solutions of lower composition, 70–75 wt%, were found useful for fabrication of high-quality cellulose nano-crystals (optimal size, crystallinity and surface charge). Reaction at high temperature at this PA content achieved hydrolysis of the amorphous regions only while phosphorylating the nanocrystal surface [58].

Contrary to these several reports indicating the relevance of some water content for cellulose dissolution by PA, the earlier studies on liquid crystallinity in cellulose/PA solutions [48] and fiber spinning from such solutions [49] reported that anhydrous phosphoric acid (P_2O_5 content above that of pure H_3PO_4, which is 72.4 wt%) is an excellent cellulose solvent. Liquid crystallinity was observed at cellulose concentrations above 7.5 wt% at room temperature in solvent P_2O_5 content of 74 wt%. A high cellulose concentration of 38 wt% could be achieved at these anhydrous conditions. Similar results were also verified in a later report [59]. Nevertheless, a recent comprehensive study of cellulose solutions in 85 wt% PA using advanced analytical techniques of cryo-transmission electron microscopy (cryo-TEM), polarization transfer solid-state nuclear magnetic resonance, and

diffusing wave spectroscopy, as well as polarized light microscopy (PLM) and mechanical rheometry, highlighted the true molecular dissolution of cellulose in PA with this water content. Both isotropic and liquid crystal states were observed, with a transition at about 7.5 wt% cellulose at 25 °C, which reverted back to the isotropic state upon heating to 60 °C [60].

Molecular dissolution of cellulose in various solvents has been studied by small-angle x-ray and neutron scattering (SAXS and SANS, respectively). The scattering pattern describes the intensity of radiation after background subtraction, $I(q)$, measured at scattering vector $q = 4\pi \sin(\theta)/\lambda$, where 2θ is the scattering angle and λ the incident wavelength. It can probe structures on the lengths scale between the cross-section of individual chains, less than 1 nm, to that of fibrils, tens of nm, and dimensions of fibrillar clusters that can range to the micrometer scale, requiring ultra-small angle scattering techniques. Dissolved cellulose chains have been considered since early studies to be semi-flexible polymer chains (SFPC) [61]. The scattering from SFPCs in dilute solution can be described by form factors (FF) derived by Pedersen and Schurtenberger (PSFF) for "worm-like" chains with and without excluded volume interactions, relevant for chains in "theta" or good solvent conditions, respectively [62]. This model was applied to SAXS measurements of cellulose dissolved in ionic liquids: a mixture of tetrabutylammonium acetate and dimethylsulfoxide [21], and 1-ethyl-3-methyl-immidazolium methyl-phosphonate [63]. Using a core-shell structure for the chain cross-section with the PSFF, the electron density profile in a cross-section perpendicular to the chain segment was derived, indicating IL solvation of the cellulose chain [21,63].

Other than applying the full PSFF, which can be quite elaborate, some characteristic features are evident directly from the scattering pattern. In the q-range of $1/l_p \lesssim q \lesssim 1/r_c$ where r_c and l_p are the radius of gyration of the chain's cross-section and its persistence length, respectively, the rod-like local structure of the chain is evident by a power law:

$$I(q) \cong Aq^{-1} \tag{1}$$

which is typical of rigid rods, where the prefactor A is related to the mass per unit length of the chain [64,65], and can be calculated by [66,67]:

$$A \cong \pi \varphi S_o (\Delta\rho)^2 \tag{2}$$

where φ is the volume fraction of rods, S_o is the rod's cross-section area and $\Delta\rho$ is the difference in the scattering length density (SLD) between the rod and solvent. Previous SANS studies of cellulose solutions in the IL 1-ethyl-3-methyl-immidazolium acetate (EMIMAc) and its mixture with dimethylformamide (DMF) relied on contrast between cellulose and deuterated EMIMAc [66] and of deuterated cellulose and protiated EMIMAc [67]. These studies demonstrated significant discrepancies between the measured values of the prefactor A and the value calculated from the cellulose chain structure, which were interpreted as due to binding of IL moieties to the cellulose chain. At somewhat higher values of q the Guinier-type approximation is appropriate [64,65]:

$$I(q) = Aq^{-1}\exp\left(-\frac{1}{2}r_c^2 q^2\right) \tag{3}$$

If significant signal is accessible at high-q, above the background and incoherent scattering, a fuller model of the chain cross-section can be evaluated, as mentioned above [21,63]. SAXS measurements from cellulose dissolved in EMImAc, before and after heating, were evaluated by Eq. (3) and using a model of coaxial double-shelled cylinders of finite length [68]. The chain's cross-section r_c in unheated solutions was found comparable to its value in the cellulose I crystal, while heating resulted in its increase, interpreted as due to release of inter-molecular hydrogen bonds and interaction with IL molecules, which also reduces the density of IL molecules in this shell of interaction [68]. It was also shown by SAXS that a small quantity of added water affects the cellulose conformation, its interaction with IL and induces aggregation [69].

The scattering at values of $q < 1/l_p$, can exhibit signs of several different effects. If inter-chain correlations can be neglected, at low concentration below that of chain overlap, an intermediate power-law behavior: $I(q) \cong Aq^{-1/\nu}$ may be observed, where ν is the Flory exponent 0.5 or 0.588 for chains without (Gaussian) or with excluded volume interactions, respectively [70]. The overlap concentration can be estimated as $c^* \simeq M/(2^{3/2}N_{AV}R_g^3)$ where M and R_g are the chain molecular weight and total radius of gyration and N_{AV} is Avogardro's number [71]. However, for semi-flexible chains such as cellulose, with increasing persistence length c^* decreases significantly [72] and the effect of inter-chain interactions reduce the intensity below that of the expected power law. For $c > c^*$ the scattering pattern can be approximated by the Ornstein-Zernike (OZ) equation [73]:

$$I(q) = I(0)/\left(1 + \xi^2 q^2\right) \tag{4}$$

for which ξ is a characteristic length-scale of inter-chain correlations ("correlation length") and $I(0) = \Delta\rho^2\varphi^2/K_{os}$, where $\Delta\rho = (\rho_p - \rho_s)$ is the difference in scattering length density between polymer and solvent (ρ_p, ρ_s, respectively), φ is the polymer volume fraction and $K_{os} = (c/RT)(d\pi/dc)$ is the osmotic modulus. R, T are the gas constant and absolute temperature, π is the osmotic pressure and c is the polymer concentration. Eq. (4) was found to be a valid approximation also for stiff polymers [74]. Conversely, enhanced excess scattering intensity at the low-q part of the scattering pattern is a characteristic of aggregation to large-scale structures, such as fibrils [75], as was demonstrated for concentrated cellulose/IL solution [17]. Thus, the absence of excess small-angle scattering and a good fit of Eq. (4) can be taken as indication of true molecular dissolution of cellulose chains [17,76]. Scaling rules of ξ and K_{os} with cellulose concentration [77] evaluated from SAXS patterns of semi-dilute cellulose/IL solutions, were close to those expected in good solvent conditions [76], which verified previous measurement of a rather large positive osmotic second virial coefficient by light scattering [17]. A persistence length of ~4.5 nm was estimated from SAXS measurements of the cellulose/IL solution [17].

SANS measurements of cellulose dissolution is well suited for solution in PA, due to the low absorption and incoherent scattering of D_3PO_4, in comparison to the high X-ray absorption of PA, and the good contrast in scattering length density (SLD) between cellulose and D_3PO_4. The objective of this study is to evaluate the role of water in dissolution of cellulose by PA, by

assessing the extent of chain aggregation as a function of water content in the PA solvent, within the narrow widow of dissolution (81–86 % PA). The actual SLD of cellulose chains dissolved in PA, due to phosphorylation, is also discussed.

Materials and methods

Materials and sample preparation

Microcrystalline cellulose was purchased from Sigma Aldrich (product no. 435,236 Lot no. MKCJ3230, Rehovot, Israel). Deuterated phosphoric acid (dPA) solution in D_2O (85 wt% dPA, product no. 176,753), phosphorous pentoxide (P_2O_5) and D_2O were also purchased from Sigma Aldrich (Rehovot, Israel). MCC powder was first dried in a vacuum oven at 60 °C and 0.26 kPa for at least 24 h. The dried MCC powder was rinsed in D_2O and then dissolved in cold (0 °C) dPA prepared in advance by mixing 85 % dPA solution with either D_2O or P_2O_5. The solution was mixed in a chiller at 0 °C by mechanical stirring at 400 rpm for 1 h. The solutions were prepared sequentially and kept in cooling (4 °C) overnight before transfer by flight to the neutron facility, at which they were stored for another day, still in cooling, until they were measured sequentially, at each sample to detector distance.

Small-angle neutron scattering (SANS) measurements

SANS measurements were carried out at the FRM-2 research reactor, at the Jülich Center for Neutron Science, Outstation at the Heinz Maier-Leibnitz Zentrum, Garching, Germany on the KWS-2 beamline [78,79]. The samples were studied in quartz cuvettes of 2 mm thickness at temperature of 25 °C. Experiments were carried out at sample to detector distances (SDD) of 2, 8, and 20 m, and collimation was positioned at the same lengths as the SDDs. A wavelength (λ) of 5 Å, with a wavelength spread $\Delta\lambda/\lambda = 20$ %, was employed, providing a range of scattering vectors q ~ 0.002–0.345 $Å^{-1}$. The data were corrected for the detector sensitivity (using an incoherent plexiglass sample). Electronic noise (using a B4C mask) and scattering from an empty cell were subtracted. Intensity calibration on the absolute scale (scattering cross section per unit volume, cm^{-1}) was performed using a plexiglass secondary standard. The measured counts from the two-dimensional detector array containing 128×128 channels were averaged radially to attain a one-dimensional scattering curve. Data reduction and initial visualization utilized the QtiKWS software [80].

Cryogenic transmission electron microscopy (cryo-TEM)

The dispersion of cellulose in PA solutions was directly-imaged by cryo-TEM imaging. Preparation of the specimen for cryo-TEM imaging was performed in a controlled environment vitrification system (CEVS) [81] at ambient temperature. A drop of the solution was placed on a TEM copper 200 mesh grid covered with a perforated carbon film (Ted Pella, Redding, CA, USA) and was immediately blotted with filter paper yielding a thin film which was rapidly vitrified by plunging into liquid nitrogen. The specimen was then transferred to the microscope using a Gatan 626 cryo-specimen holder kept at -180 °C, and transfer-station (Gatan Ametek, Pleasanton, CA USA). Imaging was performed by a Talos 200C (200 kV) high resolution TEM (Thermo Fisher Scientific Inc., Hillsboro, OR, USA), equipped with a field emission gun electron emitter. The data were collected by a Ceta 16 M, a high resolution CCD camera, or by a Falcon III direct imaging camera (Thermo Fisher Inc.) for high resolution imaging at low dose mode. Image processing was done using the TIA software (Talos images).

Results and discussions

The effect of water content in PA on SANS patterns from cellulose solutions

The solutions of 2 wt% MCC in dPA/D_2O solvents of dPA contents between 81, and 97 wt% appeared clear and transparent, whereas the solution at the lowest dPA content (78 %) was turbid. For example, images of vials containing 2 wt% cellulose solutions in 78 and 81 % dPA are presented in Fig. 1a and b, respectively. The turbidity of the former, compared to the transparent appearance of the latter are evident.

SANS measurements were performed on 2 wt% solutions of cellulose dissolved in deuterated phosphoric acid/D_2O solvent of varying PA content (78, 81, 83, 85, 87, 90, 94 and 97 wt% dPA). The patterns from six solutions in solvent compositions of 81–94 wt% dPA do not exhibit any significant difference, and thus are shown together in Fig. 2a to indicate that the structure of cellulose dissolved in these solutions is quite similar. The SANS pattern from the solution in 97 % dPA differs at low angles from that from the six solutions in 81–94 %, and that from the solution in 78 % dPA differs significantly. Thus, the SANS patterns presented in Fig. 2b are from solutions in 78 and 97 wt% dPA, in comparison with that from the solution in 85 % dPA which represents the six solutions in intermediate dPA contents. It is evident that the patterns from all solutions except the one in 78 % dPA exhibit nearly a q^{-1} power-law relation of intensity to scattering vector at the higher q-range, characteristic of rod-like structures, as was described previously for cellulose solutions in other types of good solvents. [17,21,25,30,63,66,67,76] At the lower-q range of the scattering patterns from these solutions,

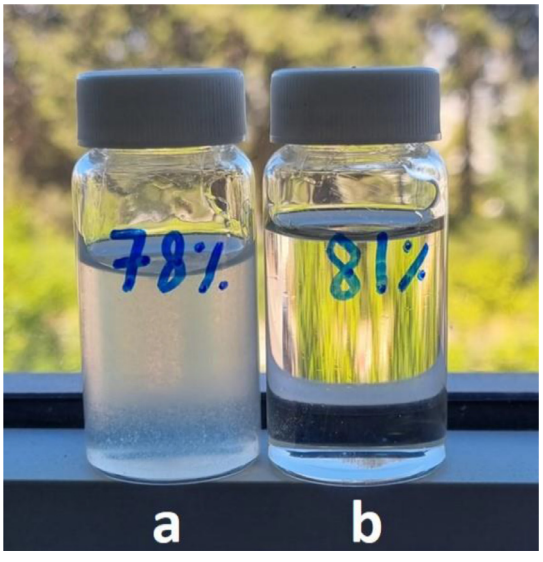

Fig. 1

Images of vials containing 2 wt% cellulose solutions in: (a) 78 and (b) 81 % PA.

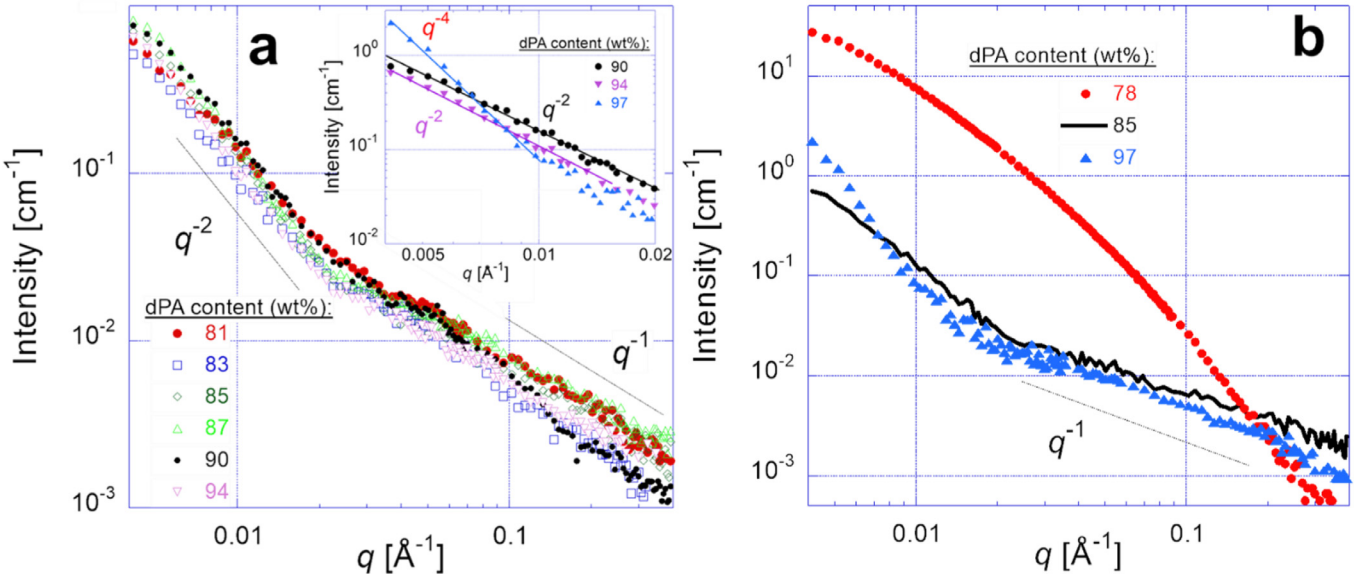

Fig. 2

SANS patterns from 2 wt% cellulose solutions in dPA/D_2O solvents composed of: (a) 81, 83, 85, 87, 90 and 94 wt% dPA, exhibiting nearly similar patterns (note, no discernible differences are meant to be demonstrated). Insert: Patterns at low-q from solution in 90, 94 and 97 %; and (b) 78, 85 and 97 wt% dPA, exhibiting dissimilar patterns (that of 85 % PA solution is repeated for comparison).

excess scattering beyond that expected from the q^{-1} power-law is observed. As mentioned above, the patterns from solutions in 81–94 wt% dPA are quite similar, and the apparent power-law at low-q in the patterns from these solutions is nearly q^{-2}, as indicated in Fig. 2a. The increased power-law at low-q can be due to inter-segmental interactions of semi-flexible chains at $q < 1/l_p$, which conform to the OZ relation, Eq. (4), at concentration above that of coil overlap (c*). Such behavior was reported for cellulose solutions in ionic liquid (1-ethyl-3-methyl imidazolium acetate – EMImAc) and its mixture with a dimethyl-formamide (DMF) at 1:9 molar ratio [76]. It was interpreted as indicating molecularly dissolved cellulose chains. The overlap concentration of cellulose from MCC as used here, dissolved in EMImAC/DMF (1:9 molar ratio), was estimated as 0.82 wt% based on viscosity [76] and light scattering measurements of its molecular parameters (M, R_g) [17]. This translates to a value of c* slightly smaller than 0.5 wt% for this cellulose dissolved in the dPA solutions under study here, considering the densities of the respective solvents and taking a value of 1.6 g/cm^3 for the cellulose density. The SANS measurements indicate that PA solutions at content of 81–94 wt% are good solvents for cellulose providing for molecular-level dissolution. The break between the -1 and -2 power-law regions indicates a persistence length about 30 Å. It should be noted that this kind of nearly -2 power-law at low-q has also been interpreted as due to random aggregation of dissolved cellulose chains in an IL having a mass-fractal structure [63], similar to simulated fractal aggregates of rigid rods, exhibiting a fractal dimension (hence scattering power-law) between 1.8 to 2.3 [82]. The actual distinction between these two interpretations (entangled semi-rigid chains and random fractal aggregates) may not be significant.

The excess scattering at low-q from the solution in 97 wt% dPA is significantly higher, with an apparent power-law about q^{-4}, as indicated in Fig. 2b. This suggests the existence of larger structures with rather sharp interfaces [83], most likely cellulose fibrils that were not molecularly dissolved. The scattering from cellulose dissolved in 78 wt% dPA is completely different, being more than an order of magnitude higher in intensity, does not exhibit an apparent two-power law pattern with exponent of -1 in the high-q range, but rather a slowly decreasing slope (on double logarithmic scales) with increasing q from about -2 to about-3. Evidently, at this high water content PA does not dissolve cellulose to individual chains but rather as cluster, which will be analyzed further below. On the other hand, at low water content, such as at 97 wt% dPA studied here, not all fibrils have been dissolved. This provides evidence from cellulose chain scattering patterns for the window of dissolution in PA ranging in acid content from about 81 to 94 wt%.

Analysis of the total scattered intensity ("invariant") at different water contents

The total (integrated) scattering intensity is related to the volume fraction (φ) of dissolved cellulose and its contrast with the solvent ($\Delta\rho$) by the Porod invariant (Q), appropriate for a two-phase system [84]:

$$Q = \int_0^\infty I(q)q^2 \mathrm{d}q = 2\pi^2(\Delta\rho)^2\varphi(1-\varphi) \quad (5)$$

Care should be taking in estimating the SLD of cellulose chains dissolved in PA, in consideration of the action of PA on AGU. Phosphorylation reactions can take several forms, but it is established that the dominant phosphorylation occurs at the $C^{(6)}$ hydroxyl [85,86]. Here we assume that one phosphate monovalent anion is attached per AGU as $–C^{(6)}–OP(O)(OH)O^-$. Cellulose phosphorylation by PA is evident on the surface of nanocrystals obtained by regeneration of MCC swollen by PA without the use of catalysts such as urea (a well known phosphorylation catalyst [85,87]), which remains even after

washing [53,88]. Furthermore, we assume that on each AGU, the two labile hydrogens on the remaining hydroxyls of the sugar ring and the one on the monovalent anionic phosphate group are fully exchanged with deuterium of the dPA/D_2O solvent (ignoring the small molar H/D ratio due to the cellulose hydroxyls incurs an error of less than 1 %). The density of phosphorylated cellulose is estimated by taking 1/4 the unit cell volume of the cellulose Iβ crystal (~658.3 Å^3) [89] adding the volume of –P(O)(OH)O^- taken as ~44 Å^3 from half the unit cell volume of disodium orthophosphite pentahydrate [90] minus the volume five water molecules and two sodium ions. The SLD of phosphorylated cellulose is thus estimated as 4×10^{-6} Å^{-2}, calculated using the approximated formula ($C_6H_7D_3O_8P$) and density ~1.9 gr/cm^3 in the usual manner [91]. Alternatively, we can consider binding of phosphate ions to AGU by hydrogen bonding as [52]: $C^{(6)}OH\cdots[OP(O)(OH)_2]^-$, for which the molar volume of the ion (31.3 cm^3/mol) [92] can be added to that of AGU, and the SLD estimated as 4.1×10^{-6} Å^{-2} ($C_6H_7D_3O_8P$). We had previously shown that ion binding from ionic liquid to cellulose dissolved in it can alter the SLD of cellulose and its contrast to the surrounding solvent [66,67]. In this analysis the SLD of the dissolved cellulose is taken as 4×10^{-6} Å^{-2}.

The SLDs of the respective solvent compositions were evaluated assuming volume additivity, by linear extrapolation between the SLD of 85 wt% dPA/D2O calculated as 5.76×10^{-6} Å^{-2} [91] using its reported density (1.736 gr/cm^3 at 25 °C [93]) and that for 100 % dPA calculated as 5.57×10^{-6} Å^{-2} [91] using the estimated density of 100 % H_3PO_4 (1.93 gr/cm^3 at 25 °C [94], and taking into account its deuteration). The solvent SLDs are tabulated in Table 1, with the estimated contrasts ($\Delta\rho$), the linear extrapolation being validated by the data of Egan and Luff [94]. The invariants were calculated by Eq. (5) with the data collected in the q-range between the first accessible data point (q_{min}=0.00413Å^{-1}) and the largest point of significant signal above the background (q_{max}=0.392Å^{-1}). The main error in invariant calculation is due to the need to extrapolate to infinite q in Eq. (5), which is significant to the q^2 wt of the high-q data. Typically, scattering patterns should decrease at high-q with a large exponent nearly q^{-4} [84], which should be expected in this case from $q>>(r_c)^{-1}$. However the current data is not sufficient for such extrapolation. Therefore a lower bound for Q was evaluated by integrating the measured data in the q-range mentioned above. Its calculated values as well as the volume fractions of dissolved cellulose, evaluated by Eq. (5) are presented in Table 1. Considering that the estimation of the volume fraction of cellulose contributing to the measured SANS signal is only a lower bound due to the lack of extrapolation to infinite-q in the invariant calculation, and the uncertainty in the estimation of the SLD of phosphorylated cellulose chains, the estimated volume fractions presented in Table 1 are indicative that as significant part of cellulose microcrystals are opened by the action of phosphoric acid at all the compositions under study, and the chains undergo phosphorylation, even if not all are dissolved as individual polymer chains.

*Analysis of the rod-like scattering at high-*q*, at different water contents*

The volume fraction of individually dissolved cellulose chains in solutions containing 81–94 wt% dPA can also be assessed by analysis of the prefactor of the q^{-1} power-law observed at high-q, by fitting Eq. (1) in the relevant q-range and applying Eq. (2). This approach is valid in two cases. If all cellulose is dissolved as individual chains, and can be viewed a persistent Kuhn chains, i.e. made of rod-like segments, then their semi-dilute solution should exhibit the q^{-1} power-law at high q turning to Eq. (4) at lower q, exhibiting a q^{-2} power-law at intermediate q, as exhibited in Fig. 2. In this case the prefactor of Eq. (1) is related to the total volume fraction of rods [74]. On the other hand, if the solution is assumed to be composed of two independent populations, dissolved chains and aggregates, the total scattering may be modeled as a sum of two independent terms, due to each population. Such assumption is widely used in analysis of polymer solutions or gels with larger-scale inhomogeneities [95], including semi-rigid polymers and their aggregates [75]. In this case the prefactor of Eq. (1) is related to the volume fraction of dissolved chains.

The q^{-1} power-law fits to the measured data are presented in Fig. 3, in the range $0.018<q<0.15$ Å^{-1}, for which reliable signal is attained above the background for significant fitting. The volume fractions are evaluated using Eq. (2) with an estimate cross-section area of 36 Å, taking into account the area per chain in the cellulose (I or II) crystal unit cell [86,89], 32 Å^2, expanded slightly due to phosphorylation as mentioned above. The estimated values, presented in Table 2, which do not rely on data extrapolation, are

Table 1

Solvent SLDs, and estimated contrast, invariants and volume fractions.

dPA content in D_2O [wt%]	dPA SLD [Å^{-2} x10^{-6}]	Contrast[(1)] ($\Delta\rho$) [Å^{-2} x10^{-6}]	Invariant[(2)] (Q) [cm^{-1}Å^{-3} x10^{-5}]	Volume fraction cellulose[(3)] (φ)
78	5.84	1.84	7.71	0.012
81	5.80	1.80	5.64	0.009
83	5.78	1.78	3.44	0.005
85	5.76	1.76	5.52	0.009
87	5.73	1.73	6.55	0.011
90	5.70	1.70	3.62	0.006
94	5.65	1.65	4.27	0.008
97	5.61	1.61	3.11	0.006

(1) Assuming the SLD of phosphorylated cellulose as 4×10^{-6} Å^{-2}.
(2) By integration as in Eq. (5) but between the limits of the measured data $0.00413<q<0.392$Å^{-1}.
(3) Estimated lower bound from the calculated invariant (Q) by Eq. (5).

Table 2

Parameters from fits of the rod-like scattering patterns to Eq. (1), and evaluated cellulose volume fractions compared to the initial values.

dPA content in D_2O wt%	Input cellulose vol. fraction [1]	Prefactor A [2] $cm^{-1}Å^{-1}$ x10^{-4}	Calc. cellulose vol. fraction [3]
81	0.022	7.5	0.023
83	0.023	5.5	0.017
85	0.023	6.0	0.019
87	0.023	6.6	0.022
90	0.024	7.0	0.024
94	0.024	5.3	0.019
97	0.025	4.3	0.017

[1] Calculated from 2 wt% cellulose, assuming cellulose density of 1.6 g/cm^3 and volume additivity of cellulose, dPA and D_2O.
[2] Calculated from fits of the rod-like scattering patterns to Eq. (1).
[3] Calculated from the fitted prefactors A using Eq. (2).

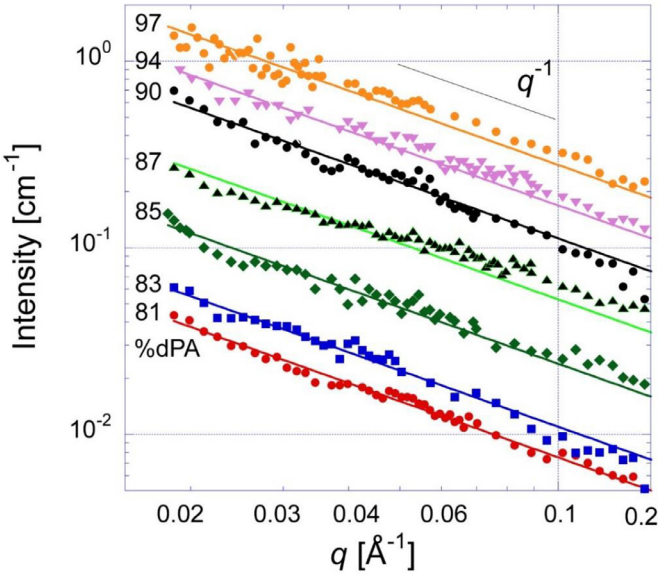

Fig. 3

The q^{-1} power-law fits (Eq. (1)) to the measured SANS patterns from 2 wt% cellulose solutions in solvent compositions of 81, 83, 85, 87, 90, 94 and 97 wt% dPA, (exhibiting nearly similar patterns). Fitting performed in the range $0.018<q<0.15$ Å^{-1}. The bottom data (of 81 % dPA solution) is actual. Each successive pattern presents data multiplied by successive factors of 2 for clarity of presentation.

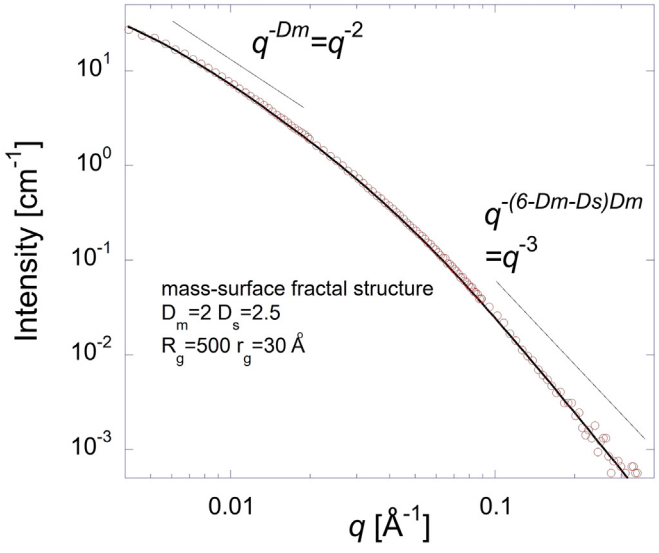

Fig. 4

SANS pattern from 2 wt% cellulose solutions in 78 % dPA solvent. Solid line is a fit of the mass-surface fractal model (Eqs. (6), (7)) with parameters as listed on the plot.

quite close to those calculated from the weight fraction of cellulose in the prepared solutions. This indicates that a significant faction of cellulose is indeed dissolved as individual chains.

The structure of cellulose solution in 78 wt% dPA

The SANS pattern from 2 wt% cellulose solution in 78 % dPA differs significantly from those at other dPA contents, both in amplitude and in shape as shown in Fig. 2b, in accord with its turbid macroscopic appearance (Fig. 1). The apparent limiting power-law behaviour is about -2 at low-q and -3 at high-q, as shown in Fig. 4. The high measured intensity yielded the high calculated volume fraction listed in Table 1 for this solution, derived by Eq. (5) even without data extrapolation. This was interpreted above as indicating that most of the cellulose chains are phosphorylated and released from the crystal, even if not dissolved molecularly. The shape of the scattering pattern is reminiscent of that which appears in mass-surface fractal such as aerosol aggregates, in which primary particles with an irregular surface structure ("surface fractal"), of average gyration radius r_g, are aggregated to larger irregular structures ("mass fractals") of average gyration radius R_g. The scattering from such structures may be modelled as [96,97]:

$$I(q) = I(0)\left\{\left[\left(1+b^2q^2\right)\right]^{D_m/2}\left[\left(1+a^2q^2\right)\right]^{(6-D_s-D_m)/2)}\right\}^{-1} \quad (6)$$

Where D_s and D_m are the surface and mass fractal dimensions, and a and b are size characteristics of the primary and aggregated structures, respectively, related to their respective gyration radii by:

$$a = r_g/[3(6-D_m-D_s/2)]^{1/2} \quad (7a)$$

$$b = R_g/(3D_m/2)^{1/2} \quad (7b)$$

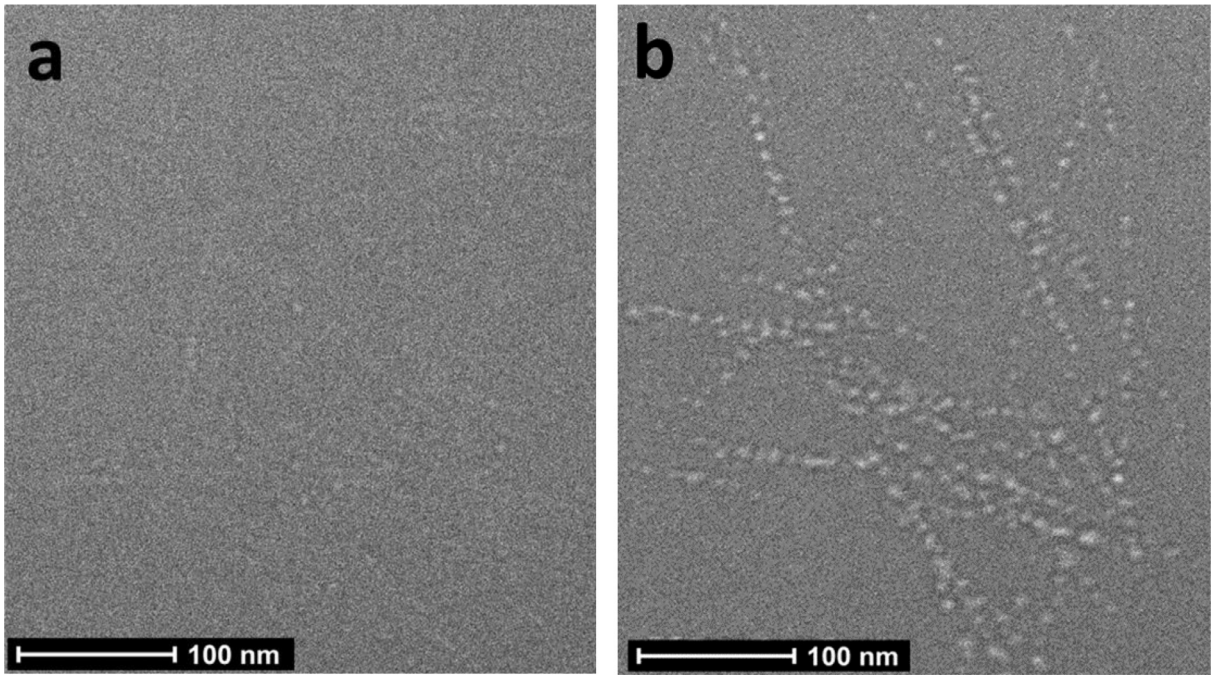

Fig. 5

CryoTEM images of cellulose solutions in 78 % PA: (a) taken with a low dose of electron radiation (~3.9 $e^-/Å^2$), and (b) taken with a higher dose (~5.2 $e^-/Å^2$).

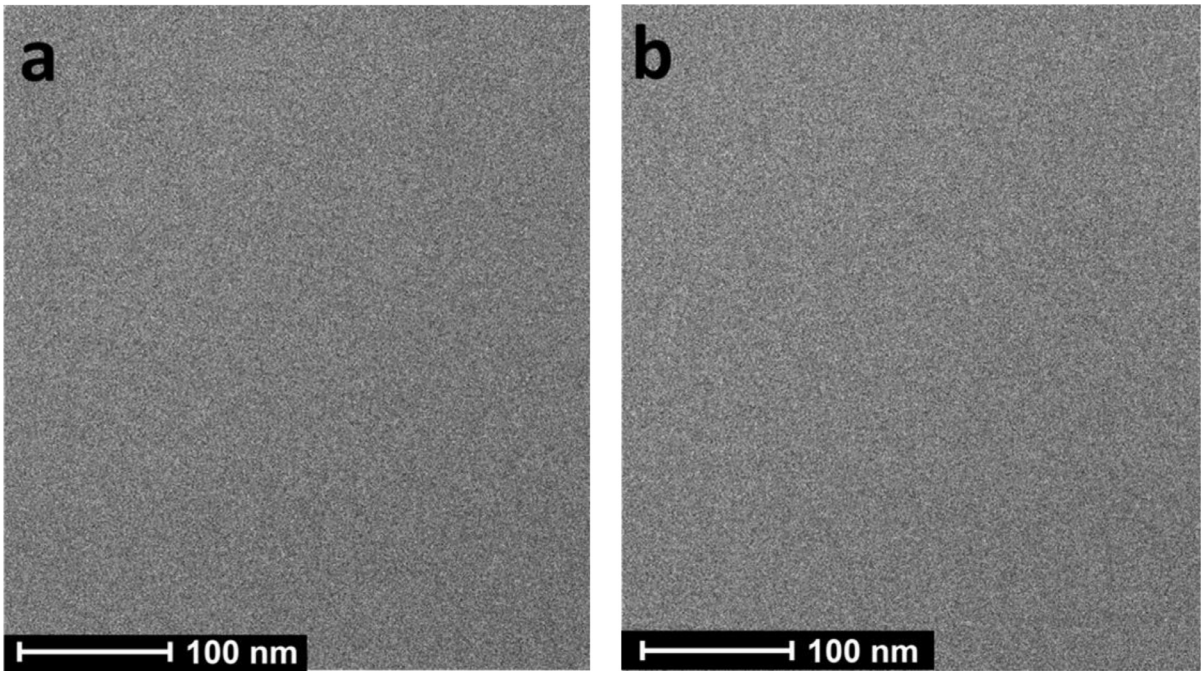

Fig. 6

CryoTEM images of cellulose solutions in 81 % PA: (a) taken with a dose of electron radiation ~5.5 $e^-/Å^2$, and (b) taken with a higher dose (~16.4 $e^-/Å^2$).

Eq. (6) was applied to the SANS pattern of 2 wt% cellulose in 78 % dPA, as shown in Fig. 4, by taking the limiting power law at low-q as the mass fractal dimensions ($D_m = 2$). Apparently the size of the aggregated structure is too large for the resolution of the measurement ($b \gtrsim q_{min}^{-1} \approx 240$ Å). Thus we arbitrarily assign a value of $b = 500$ Å. Thus, the fitted parameters of Eq. (6) are $I(0)$ and the characteristics of the primary particles: size a (or r_g) and surface fractal dimension D_s. A good fit of the data, as shown in Fig. 4, is obtained with $D_s = 2.5$ and $r_g = 30$ Å. This result may be interpreted as indicating that the MCC crystals have been dissolved by the action of PA, yet, some elementary fibril structure remains, having an irregular surface due to partially dissolved

cellulose chains. These surface features present a surface fractal dimension (2.5), and may be assumed to be composed of segments emanating from partially dissolved fibrils, forming smaller-scale structures of gyration radius ~30 Å [82].

Indication of disordered aggregates of rod-like fibrils, with possible fractal appearance, may be gleamed in images of the 2 wt% cellulose solution in 78 % PA obtained by cryo-TEM, displayed in Fig. 5. Due to the electron-beam radiation sensitivity of the cellulose solutions, and electron absorption by PA, it was rather difficult to obtain an image free of radiation damage. Fig. 5a presents an image with minimal damage (electron dose ~3.9 $e^-/Å^2$), in which faint light streaks may be discerned, possibly indicating the lighter cellulose fibrils against the background of the darker-appearing vitrified PA. Electron radiolysis often initiates at the dispersed organic matter in the vitrified inorganic media, e.g., water [98,99] or acid [100,101], as was also observed in cellulose/PA solution [60]. Thus, the bubble-like structures that appear in Fig. 5b, due to radiation damage as the image was recorded at higher exposure (~5.2 $e^-/Å^2$), are considered to be due to radiolysis at the interface of acid - cellulose fibrils. This is a similar experimental approach to that taken in imaging carbon nanotubes (CNTs) in chlorosulfonic acid [100], where direct radiation damage was applied to detect the CNTs. The enhanced contrast highlights the structure of interconnected fibrils that may be assumed to be part of a fractal-like structure on a larger scale. For comparison, images of the solution in 81 % PA are shown in Fig. 6. The image taken with exposure to an electron dose of ~5.5 e^-/A^2, shown in Fig. 6a, as well as the one shown in Fig. 6b, taken at a higher dose (~16.4 e^-/A^2), even much higher that used for the image in Fig. 5b, do not exhibit any discernible fibrillar structure. This supports the SANS results indicating molecular dissolution of cellulose chains in 81 % PA solvent.

Analysis of the SANS patterns from cellulose solutions of different concentrations

The effect of cellulose concentration on the scattering patterns was studied with solutions in 83 wt% dPA, containing 0.5, 1, 2 and 4 wt% cellulose, as presented in Fig. 7a. All patterns exhibit a similar shape, with the limiting power laws of q^{-1} at high-q and about q^{-2} at low-q. The evaluated scattering invariants, again calculated without data extrapolation to infinite q as described above, with the associated cellulose volume fractions calculated from them, are presented in Table 3, as are the fits at high-q of the rod-like pattern (Eq. (1)), shown in Fig. 7b, and

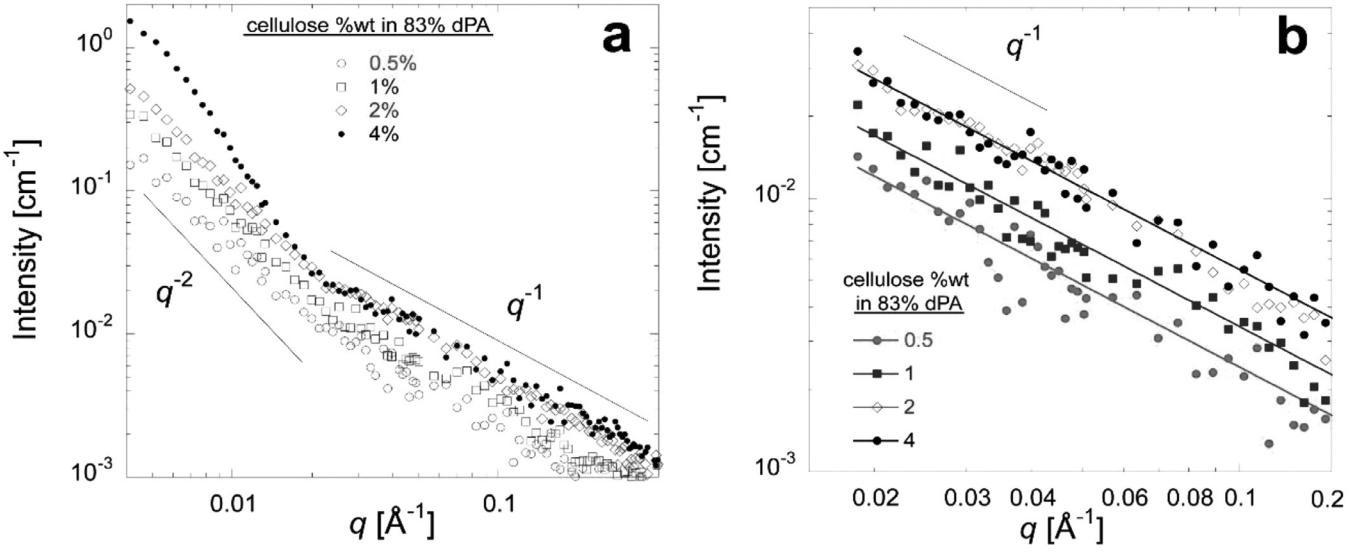

Fig. 7

(a) SANS patterns from cellulose solutions in 83 % dPA, containing 0.5, 1, 2 and 4 wt% cellulose. (b) Fits of the q^{-1} power-law (Eq. (1)).

Table 3

The effect of cellulose concentration on parameters calculated from the SANS patterns of solutions in 83 % dPA.

Cellulose content wt%	Input cellulose volume fraction	Fitted prefactor (*A*)[(1)]		Calculated invariant (*Q*)[(3)]	
		$cm^{-1}Å^{-1}$ x10^{-4}	volume fraction[(2)]	$cm^{-1}Å^{-3}$ x10^{-5}	volume fraction[(4)]
0.5	0.0055	2.4	0.006	1.58	0.0025
1.0	0.0115	3.4	0.009	2.40	0.0038
2.0	0.023	5.5	0.015	3.44	0.0055
4.0	0.046	5.5	0.015	4.23	0.0068

(1) Calculated from fits of the rod-like scattering patterns to Eq. (1).
(2) Calculated from the fitted prefactors *A* using Eq. (2).
(3) By integration as in Eq. (5) but between the limits of the measured data $0.00413 < q < 0.392 Å^{-1}$.
(4) Estimated lower bound from the calculated invariant (*Q*) by Eq. (5).

the volume fractions calculated from the fitted prefactors. The volume fractions from the invariant calculations are significant under-estimations but those estimated from the prefactors of the rodlike scattering are quite comparable to the input values, indicating again that a significant part of the cellulose chains are dispersed from the tight crystals, more so at the lowest cellulose composition. However, when the concentrated is doubled from 2 to 4 wt%, the fraction of dissolved cellulose is not changed. This may indicate that at 4 wt% cellulose there is no significant increase in the volume fraction of individually dissolved cellulose chains, which is in accord with the observation of aggregate scattering at low-q.

Conclusions

Small-angle neutron scattering (SANS) measurements were used to assess the state of dissolution of cellulose chains in deuterated phosphoric acid (dPA) at water contents from 78 to 97 % water. dPA/D_2O mixtures were utilized due to sufficient contrast with cellulose, low incoherent scattering cross-section and low radiation absorption compared to x-rays. The action of phosphoric acid on cellulose crystals disrupts intra- and inter-molecular hydrogen bonds resulting in disruption of the tight crystal structure at all dPA/D_2O compositions studied. SANS provides evidence that a significant part of the cellulose chains are molecularly dissolved as individual chains, in 2 wt% cellulose solutions, at water content of 81–94 wt%, with insignificant difference between solvents of the various water compositions. At 97 % dPA evidence for a small content of undissolved fibrils is also noted. Increasing cellulose content to 4 wt% in 85 % dPA shows no significant increase in the volume fraction of individually dissolved cellulose chains, which is in accord with the observation of aggregate scattering at low-q. Dissolution in 78 % dPA exhibits a marked difference in the scattering pattern. The intensity is significantly higher, without a noticeable break in the apparent power law behavior, and does not exhibit the q^{-1} power law at high-q. The SANS pattern can be fitted by the mass-surface fractal model, possibly due to existence of small fibrils with an irregular (rough) surface, likely caused by chain segments emanating from partially dissolved fibrils, which form larger "open" structures as networks or mass fractals with a low dimension (~2).

The rather wide window of water content in PA (~81–94 %), in which cellulose dissolves similarly, irrespective of water content, may be rationalized by a combination of complementary effects. Decreasing water content below 20 wt% enhances PA activity towards both cellulose wettability [51,52] and phosphorylation reaction [85], yet significantly increases the solvent viscosity [102]. Thus a combination of thermodynamic and kinetic effects can rationalize the origin of the main finding of this study.

Declaration of competing interest

The authors declare the following financial interests/personal relationships which may be considered as potential competing interests:

Yachin Cohen reports financial support, equipment, drugs, or supplies, and travel were provided by Technion Israel Institute of Technology.

Data availability

Data will be made available on request.

CRediT authorship contribution statement

Gilad Alfassi: Data curation, Investigation, Writing – review & editing. **Aurel Radulescu:** Data curation, Formal analysis, Software, Writing – review & editing. **Sapir Lifshiz-Simon:** Visualization, Writing – review & editing. **Sapir Rappoport:** Visualization, Writing – review & editing. **Yachin Cohen:** Conceptualization, Formal analysis, Funding acquisition, Supervision, Writing – original draft, Writing – review & editing.

Acknowledgments

This project was funded by the Israel Science Foundation Grant no. 123/18. This work is based upon experiments performed at the KWS-2 instrument operated by JCNS at the Heinz Maier-Leibnitz Zentrum (MLZ), Garching, Germany. G.A. and Y.C. gratefully acknowledge the financial support provided by JCNS to perform the neutron scattering measurements at the Heinz Maier-Leibnitz Zentrum (MLZ), Garching, Germany. This work benefited from the use of the SasView application, originally developed under NSF award DMR-0520547. SasView contains the code developed with funding from the European Union's Horizon 2020 research and innovation program under the SINE2020 project, grant agreement no 654000. (http://www.sasview.org/). We thank Prof. Y. (Ishi) Talmon for helpful discussions on cryo-TEM imaging.

References

[1] S. Raza, E. Ghasali, M. Raza, C. Chen, B. Li, Y. Orooji, H. Lin, C. Karaman, H. Karimi Maleh, N. Erk, Advances in technology and utilization of natural resources for achieving carbon neutrality and a sustainable solution to neutral environment, Environ. Res. 220 (2023), doi:10.1016/j.envres.2022.115135.

[2] D. Klemm, B. Heublein, H.P. Fink, A. Bohn, Cellulose: fascinating biopolymer and sustainable raw material, Angew. Chem. Int. Ed. 44 (2005) 3358–3393, doi:10.1002/anie.200460587.

[3] A.B. Culaba, A.P. Mayol, J.L.G. San Juan, A.T. Ubando, A.A. Bandala, R.S. Concepcion, M. Alipio, W.H. Chen, P.L. Show, J.S. Chang, Design of biorefineries towards carbon neutrality: a critical review, Bioresour. Technol. 369 (2023), doi:10.1016/j.biortech.2022.128256.

[4] B. Medronho, A. Romano, M.G. Miguel, L. Stigsson, B. Lindman, Rationalizing cellulose (in)solubility: reviewing basic physicochemical aspects and role of hydrophobic interactions, Cellulose 19 (2012) 581–587, doi:10.1007/s10570-011-9644-6.

[5] W.G. Glasser, R.H. Atalla, J. Blackwell, M.M. Brown, W. Burchard, A.D. French, D.O. Klemm, Y. Nishiyama, About the structure of cellulose: debating the Lindman hypothesis, Cellulose 19 (2012) 589–598, doi:10.1007/s10570-012-9691-7.

[6] B. Medronho, B. Lindman, Competing forces during cellulose dissolution: from solvents to mechanisms, Curr. Opin. Colloid Interface Sci. 19 (2014) 32–40, doi:10.1016/j.cocis.2013.12.001.

[7] B. Lindman, B. Medronho, L. Alves, C. Costa, H. Edlund, M. Norgren, The relevance of structural features of cellulose and its interactions to dissolution, regeneration, gelation and plasticization phenomena, Phys. Chem. Chem. Phys. 19 (2017) 23704–23718, doi:10.1039/c7cp02409f.

[8] A. Zoghlami, G. Paës, Lignocellulosic biomass: understanding recalcitrance and predicting hydrolysis, Front. Chem. 7 (2019) 874, doi:10.3389/fchem.2019.00874.

[9] M. Kostag, M. Gericke, T. Heinze, O.A. El Seoud, Twenty-five years of cellulose chemistry: innovations in the dissolution of the biopolymer and its transformation into esters and ethers, Cellulose 26 (2019) 139–184, doi:10.1007/s10570-018-2198-0.

[10] P. Alexandridis, M. Ghasemi, E.P. Furlani, M. Tsianou, Solvent processing of cellulose for effective bioresource utilization, Curr. Opin. Green Sustain. Chem. 14 (2018) 40–52, doi:10.1016/j.cogsc.2018.05.008.

[11] S. Acharya, S. Liyanage, N. Abidi, P. Parajuli, S.S. Rumi, J.L. Shamshina, Utilization of cellulose to its full potential: a review on cellulose dissolution, regeneration, and applications, Polymers 13 (2021), doi:10.3390/polym13244344.

[12] R.P. Swatloski, S.K. Spear, J.D. Holbrey, R.D. Rogers, Dissolution of cellose with ionic liquids, J. Am. Chem. Soc. 124 (2002) 4974–4975, doi:10.1021/ja025790m.

[13] R. Rinaldi, Instantaneous dissolution of cellulose in organic electrolyte solutions, Chem. Commun. 47 (2011) 511–513, doi:10.1039/c0cc02421j.

[14] H. Wang, G. Gurau, R.D. Rogers, Ionic liquid processing of cellulose, Chem. Soc. Rev. 41 (2012) 1519–1537, doi:10.1039/c2cs15311d.

[15] J. Zhang, J. Wu, J. Yu, X. Zhang, J. He, J. Zhang, Application of ionic liquids for dissolving cellulose and fabricating cellulose-based materials: state of the art and future trends, Mater. Chem. Front. 1 (2017) 1273–1290, doi:10.1039/c6qm00348f.

[16] A.H. Bhat, I. Khan, M.A. Usmani, R. Umapathi, S.M.Z. Al-Kindy, Cellulose an ageless renewable green nanomaterial for medical applications: an overview of ionic liquids in extraction, separation and dissolution of cellulose, Int. J. Biol. Macromol. 129 (2019) 750–777, doi:10.1016/j.ijbiomac.2018.12.190.

[17] D.M. Rein, R. Khalfin, N. Szekely, Y. Cohen, True molecular solutions of natural cellulose in the binary ionic liquid-containing solvent mixtures, Carbohydr. Polym. 112 (2014), doi:10.1016/j.carbpol.2014.05.059.

[18] R.C. Remsing, R.P. Swatloski, R.D. Rogers, G. Moyna, Mechanism of cellulose dissolution in the ionic liquid 1-n-butyl-3- methylimidazolium chloride: a 13C and 35/37Cl NMR relaxation study on model systems, Chem. Commun. (2006) 1271–1273, doi:10.1039/b600586c.

[19] M. Kostag, T. Liebert, O.A. El Seoud, T. Heinze, Efficient cellulose solvent: quaternary ammonium chlorides, Macromol. Rapid Commun. 34 (2013) 1580–1584, doi:10.1002/marc.201300497.

[20] J. Miao, H. Sun, Y. Yu, X. Song, L. Zhang, Quaternary ammonium acetate: an efficient ionic liquid for the dissolution and regeneration of cellulose, RSC Adv. 4 (2014) 36721–36724, doi:10.1039/c4ra06258b.

[21] A. Idström, L. Gentile, M. Gubitosi, C. Olsson, B. Stenqvist, M. Lund, K.E. Bergquist, U. Olsson, T. Köhnke, E. Bialik, On the dissolution of cellulose in tetrabutylammonium acetate/dimethyl sulfoxide: a frustrated solvent, Cellulose 24 (2017) 3645–3657, doi:10.1007/s10570-017-1370-2.

[22] Y.B. Huang, P.P. Xin, J.X. Li, Y.Y. Shao, C.B. Huang, H. Pan, Room-temperature dissolution and mechanistic investigation of cellulose in a tetra-butylammonium acetate/dimethyl sulfoxide system, ACS Sustain. Chem. Eng. 4 (2016) 2286–2294, doi:10.1021/acssuschemeng.5b01749.

[23] W. Wei, F. Meng, Y. Cui, M. Jiang, Z. Zhou, Room temperature dissolution of cellulose in tetra-butylammonium hydroxide aqueous solvent through adjustment of solvent amphiphilicity, Cellulose 24 (2017) 49–59, doi:10.1007/s10570-016-1113-9.

[24] B. Medronho, A. Pereira, H. Duarte, L. Gentile, A.M. Rosa da Costa, A. Romano, U. Olsson, Probing cellulose–solvent interactions with self-diffusion NMR: onium hydroxide concentration and co-solvent effects, Carbohydr. Polym. 303 (2023), doi:10.1016/j.carbpol.2022.120440.

[25] M.A. Behrens, J.A. Holdaway, P. Nosrati, U. Olsson, On the dissolution state of cellulose in aqueous tetrabutylammonium hydroxide solutions, RSC Adv. 6 (2016) 30199–30204, doi:10.1039/C6RA03547G.

[26] M. Gubitosi, H. Duarte, L. Gentile, U. Olsson, B. Medronho, On cellulose dissolution and aggregation in aqueous tetrabutylammonium hydroxide, Biomacromolecules 17 (2016) 2873–2881, doi:10.1021/acs.biomac.6b00696.

[27] M. Egal, T. Budtova, P. Navard, Structure of Aqueous Solutions of Microcrystalline Cellulose/Sodium Hydroxide below 0°C and the Limit of Cellulose Dissolution, Biomacromolecules 8 (2007) 2282–2287, doi:10.1021/bm0702399.

[28] T. Budtova, P. Navard, Cellulose in NaOH–water based solvents: a review, Cellulose 23 (2016) 5–55, doi:10.1007/s10570-015-0779-8.

[29] H. Qi, Q. Yang, L. Zhang, T. Liebert, T. Heinze, The dissolution of cellulose in NaOH-based aqueous system by two-step process, Cellulose 18 (2011) 237–245, doi:10.1007/s10570-010-9477-8.

[30] B. Martin-Bertelsen, E. Andersson, T. Köhnke, A. Hedlund, L. Stigsson, U. Olsson, Revisiting the dissolution of cellulose in NaOH as "Seen" by X-rays, Polymers 12 (2020), doi:10.3390/polym12020342.

[31] J. Cai, L. Zhang, Rapid dissolution of cellulose in LiOH/urea and NaOH/urea aqueous solutions, Macromol. Biosci. 5 (2005) 539–548, doi:10.1002/mabi.200400222.

[32] Z. Jiang, Y. Fang, J. Xiang, Y. Ma, A. Lu, H. Kang, Y. Huang, H. Guo, R. Liu, L. Zhang, Intermolecular interactions and 3D structure in cellulose-NaOH-urea aqueous system, J. Phys. Chem. B 118 (2014) 10250–10257, doi:10.1021/jp501408e.

[33] B. Xiong, P. Zhao, K. Hu, L. Zhang, G. Cheng, Dissolution of cellulose in aqueous NaOH/urea solution: role of urea, Cellulose 21 (2014) 1183–1192, doi:10.1007/s10570-014-0221-7.

[34] Z. Jiang, Y. Fang, Y. Ma, M. Liu, R. Liu, H. Guo, A. Lu, L. Zhang, Dissolution and metastable solution of cellulose in NaOH/Thiourea at 8 °C for construction of nanofibers, J. Phys. Chem. B 121 (2017) 1793–1801, doi:10.1021/acs.jpcb.6b10829.

[35] A.S. Bommarius, A. Katona, S.E. Cheben, A.S. Patel, A.J. Ragauskas, K. Knudson, Y. Pu, Cellulase kinetics as a function of cellulose pretreatment, Metab. Eng. 10 (2008) 370–381, doi:10.1016/j.ymben.2008.06.008.

[36] C.H. Kuo, C.K. Lee, Enhancement of enzymatic saccharification of cellulose by cellulose dissolution pretreatments, Carbohydr. Polym. 77 (2009) 41–46, doi:10.1016/j.carbpol.2008.12.003.

[37] M. Ouellet, S. Datta, D.C. Dibble, P.R. Tamrakar, P.I. Benke, C. Li, S. Singh, K.L. Sale, P.D. Adams, J.D. Keasling, B.A. Simmons, B.M. Holmes, A. Mukhopadhyay, Impact of ionic liquid pretreated plant biomass on Saccharomyces cerevisiae growth and biofuel production, Green Chem. 13 (2011) 2743–2749, doi:10.1039/c1gc15327g.

[38] Y.S. Uju, A. Nakamoto, M. Goto, W. Tokuhara, Y. Noritake, S. Katahira, N. Ishida, K. Nakashima, C. Ogino, N. Kamiya, Short time ionic liquids pretreatment on lignocellulosic biomass to enhance enzymatic saccharification, Bioresour. Technol. 103 (2012) 446–452, doi:10.1016/j.biortech.2011.10.003.

[39] X. Meng, A.J. Ragauskas, Recent advances in understanding the role of cellulose accessibility in enzymatic hydrolysis of lignocellulosic substrates, Curr. Opin. Biotechnol. 27 (2014) 150–158, doi:10.1016/j.copbio.2014.01.014.

[40] J. Rabha, S.P. Devi, S. Das, N. Roy, D.K. Jha, Microbial conversion of biomass to value-added chemicals, in: Value-Addition in Agri-Food Industry Waste Through Enzyme Technology, Elsevier, 2023, pp. 37–64, doi:10.1016/B978-0-323-89928-4.00018-3.

[41] Z. Ling, S. Chen, X. Zhang, F. Xu, Exploring crystalline-structural variations of cellulose during alkaline pretreatment for enhanced enzymatic hydrolysis, Bioresour. Technol. 224 (2017) 611–617, doi:10.1016/j.biortech.2016.10.064.

[42] S. Nagarajan, N.C. Skillen, J.T.S. Irvine, L.A. Lawton, P.K.J. Robertson, Cellulose II as bioethanol feedstock and its advantages over native cellulose, Renew. Sustain. Energy Rev. 77 (2017) 182–192, doi:10.1016/j.rser.2017.03.118.

[43] G.W. Miles, C. Dreyfus, Improvements in phosphoric acid solutions of cellulose, GB263810A, 1927.

[44] A.J. Stamm, W.E. Cohen, The viscosity of cellulose in phosphoric acid solutions, J. Phys. Chem. 42 (1938) 921–933, doi:10.1021/j100902a004.

[45] A. Ekenstam, Über das Verhalten der Cellulose in Mineralsäure-Lösungen, I. Mitteil.: die Bestimmung des Molekular-gewichts in Phosphorsäure-Lösung, Ber. Dtsch. Chem. Ges. 69 (1936) 549–552 (A and B Series), doi:10.1002/cber.19360690314.

[46] C.S. Walseth, The influence of the fine structure of cellulose on the action of cellulases, TAPPI 35 (1952) 233–238.

[47] S.P.S. Chundawat, G. Bellesia, N. Uppugundla, L. Da Costa Sousa, D. Gao, A.M. Cheh, U.P. Agarwal, C.M. Bianchetti, G.N. Phillips, P. Langan, V. Balan, S. Gnanakaran, B.E. Dale, Restructuring the crystalline cellulose hydrogen bond network enhances its depolymerization rate, J. Am. Chem. Soc. 133 (2011) 11163–11174, doi:10.1021/ja2011115.

[48] H. Boerstoel, H. Maatman, J.B. Westerink, B.M. Koenders, Liquid crystalline solutions of cellulose in phosphoric acid, Polymer 42 (2001) 7371–7379, doi:10.1016/S0032-3861(01)00210-5.

[49] M.G. Northolt, H. Boerstoel, H. Maatman, R. Huisman, J. Veurink, H. Elzerman, The structure and properties of cellulose fibres spun from an anisotropic phosphoric acid solution, Polymer 42 (2001) 8249–8268, doi:10.1016/S0032-3861(01)00211-7.

[50] X. Jia, Y. Chen, C. Shi, Y. Ye, P. Wang, X. Zeng, T. Wu, Preparation and characterization of cellulose regenerated from phosphoric acid, J. Agric. Food Chem. 61 (2013) 12405–12414, doi:10.1021/jf4042358.

[51] V.V. Vinogradov, L.N. Mizerovskii, O.P. Akaev, Reaction of cellulose with aqueous solutions of orthophosphoric acid, Fibre Chem. 34 (2002) 167–171, doi:10.1023/A:1020558829106.

[52] L.N. Mizerovskii, V.V. Afanas'eva, Reaction of cellulose with aqueous solutions of orthophosphoric acid. Structural and chemical aspects of the reaction of H3PO4 with hydrated cellulose film, Fibre Chem. 34 (2002) 329–334, doi:10.1023/A:1022150816545.

[53] J. Zhang, J. Zhang, L. Lin, T. Chen, J. Zhang, S. Liu, Z. Li, P. Ouyang, Dissolution of microcrystalline cellulose in phosphoric acid-molecular changes and kinetics, Molecules. 14 (2009) 5027–5041, doi:10.3390/molecules14125027.

[54] X. Hao, W. Shen, Z. Chen, J. Zhu, L. Feng, Z. Wu, P. Wang, X. Zeng, T. Wu, Self-assembled nanostructured cellulose prepared by a dissolution and regeneration process using phosphoric acid as a solvent, Carbohydr. Polym. 123 (2015) 297–304, doi:10.1016/j.carbpol.2015.01.055.

[55] Y.H.P. Zhang, J. Cui, L.R. Lynd, L.R. Kuang, A transition from cellulose swelling to cellulose dissolution by o-phosphoric acid: evidence from enzymatic hydrolysis and supramolecular structure, Biomacromolecules 7 (2006) 644–648, doi:10.1021/bm050799c.

[56] B.J. Watson, B. Hammouda, R.M. Briber, S.W. Hutcheson, Influence of organic liquids on the nanostructure of precipitated cellulose, J. Appl. Polym. Sci. 127 (2013) 2620–2627, doi:10.1002/app.37540.

[57] I.V. Tyshkunova, D.G. Chukhchin, I.V. Gofman, D.N. Poshina, Y.A. Skorik, Cellulose cryogels prepared by regeneration from phosphoric acid solutions, Cellulose 28 (2021) 4975–4989, doi:10.1007/s10570-021-03851-5.

[58] O.M. Vanderfleet, D.A. Osorio, E.D. Cranston, Optimization of cellulose nanocrystal length and surface charge density through phosphoric acid hydrolysis, Philos. Trans. R. Soc. A Math. Phys. Eng. Sci. 376 (2017) 20170041, doi:10.1098/rsta.2017.0041.

[59] R. Xiong, F. Li, J. Yu, P. Hu, Z. Liu, Y.L. Hsieh, Investigations on solution of cellulose in complex phosphoric acid solvent and its stability, Cellul. Chem. Technol. 47 (2013) 153–163.

[60] L. Alves, B. Medronho, A. Filipe, A. Romano, M.G. Rasteiro, B. Lindman, D. Topgaard, I. Davidovich, Y. Talmon, Revisiting the dissolution of cellulose in H3PO4(aq) through cryo-TEM, PTssNMR and DWS, Carbohydr. Polym. 252 (2021), doi:10.1016/j.carbpol.2020.117122.

[61] K. Kamide, M. Saito, H. Suzuki, Persistence length of cellulose and cellulose derivatives in solution, Die Makromol. Chem. Rapid Commun. 4 (1983) 33–39, doi:10.1002/marc.1983.030040108.

[62] J.S. Pedersen, P. Schurtenberger, Scattering functions of semiflexible polymers with and without excluded volume effects, Macromolecules 29 (1996) 7602–7612, doi:10.1021/ma9607630.

[63] K. Hirosawa, K. Fujii, K. Hashimoto, M. Shibayama, Solvated structure of cellulose in a phosphonate-based ionic liquid, Macromolecules 50 (2017) 6509–6517, doi:10.1021/acs.macromol.7b01138.

[64] V. Luzzati, Interprétation des mesures absolues de diffusion centrale des rayons X en collimation ponctuelle ou linéaire: solutions de particles globulaires et de batonnets, Acta Crystallogr. 13 (1960) 939–945, doi:10.1107/S0365110X60002284.

[65] R.P. Hjelm Jnr, The small-angle approximation of X-ray and neutron scatter from rigid rods of non-uniform cross section of finite length, J. Appl. Crystallogr. 18 (1985) 452–460, doi:10.1107/S0021889885010706.

[66] V.S. Raghuwanshi, Y. Cohen, G. Garnier, C.J. Garvey, R.A. Russell, T. Darwish, G. Garnier, Cellulose dissolution in ionic liquid: ion binding revealed by neutron scattering, Macromolecules 51 (2018) 7649–7655, doi:10.1021/acs.macromol.8b01425.

[67] V.S. Raghuwanshi, Y. Cohen, G. Garnier, C.J. Garvey, G. Garnier, Deuterated bacterial cellulose dissolution in ionic liquids, Macromolecules 54 (2021) 6982–6989, doi:10.1021/acs.macromol.1c00833.

[68] M. Koide, I. Wataoka, H. Urakawa, K. Kajiwara, U. Henniges, T. Rosenau, Intrinsic characteristics of cellulose dissolved in an ionic liquid: the shape of a single cellulose molecule in solution, Cellulose 26 (2019) 2233–2242, doi:10.1007/s10570-018-02238-3.

[69] M. Koide, H. Urakawa, K. Kajiwara, T. Rosenau, I. Wataoka, Influence of water on the intrinsic characteristics of cellulose dissolved in an ionic liquid, Cellulose 27 (2020) 7389–7398, doi:10.1007/s10570-020-03323-2.

[70] J.S. Higgins, H. Benoît, Polymers and Neutron Scattering, Clarendon Press, Oxford, 1994.

[71] J. Des Cloizeaux, G. Jannink, Polymers in Solution : Their Modelling and Structure, Clarendon Press, Oxford, 1990.

[72] A.R. Khokhlov, Phase diagram of an isotropic solution of semi-flexible macromolecules in the vicinity of the theta temperature, Polym. Sci. USSR 20 (1978) 3087–3098, doi:10.1016/0032-3950(78)90526-9.

[73] M. Daoud, J.P. Cotton, B. Farnoux, G. Jannink, G. Sarma, H. Benoit, C. Duplessix, C. Picot, P.G. de Gennes, Solutions of flexible polymers. Neutron experiments and interpretation, Macromolecules 8 (1975) 804–818, doi:10.1021/ma60048a024.

[74] T. Shimada, M. Doi, K. Okano, Concentration fluctuation of stiff polymers. I. Static structure factor, J. Chem. Phys. 88 (1988) 2815–2821, doi:10.1063/1.454016.

[75] J.J. Kwok, K.S. Park, B.B. Patel, R. Dilmurat, D. Beljonne, X. Zuo, B. Lee, Y. Diao, Understanding solution state conformation and aggregate structure of conjugated polymers via small angle X-ray scattering, Macromolecules 55 (2022) 4353–4366, doi:10.1021/acs.macromol.1c02449.

[76] S. Napso, D.M. Rein, R. Khalfin, Y. Cohen, Semidilute solution structure of cellulose in an ionic liquid and its mixture with a polar organic co-solvent studied by small-angle X-ray scattering, J. Polym. Sci. B Polym. Phys. 55 (2017), doi:10.1002/polb.24337.

[77] P.G. de Gennes, Scaling Concepts in Polymer Physics, Cornell University Press, Ithaca, N.Y., 1979.

[78] A. Radulescu, V. Pipich, H. Frielinghaus, M.S. Appavou, KWS-2, the high intensity /wide Q -range small-angle neutron diffractometer for soft-matter and biology at FRM II, J. Phys. Conf. Ser. 351 (2012) 12026, doi:10.1088/1742-6596/351/1/012026.

[79] A. Radulescu, N.K. Szekely, M.S. Appavou, KWS-2: small angle scattering diffractometer, J. Large-Scale Res. Facil. JLSRF 1 (2015), doi:10.17815/jlsrf-1-27.

[80] V. Pipich, QtiKWS, Jülich Centre for Neutron Science., (2019). http://www.qtikws.de (accessed December 28, 2022).

[81] J.R. Bellare, H.T. Davis, L.E. Scriven, Y. Talmon, Controlled environment vitrification system: an improved sample preparation technique, J. Electron Microsc. Tech. 10 (1988) 87–111, doi:10.1002/jemt.1060100111.

[82] A. Mohraz, D.B. Moler, R.M. Ziff, M.J. Solomon, Effect of monomer geometry on the fractal structure of colloidal rod aggregates, Phys. Rev. Lett. 92 (2004) 155503, doi:10.1103/PhysRevLett.92.155503.

[83] O. Glatter, O. Kratky, Small Angle X-ray Scattering, Academic Press, 1982.

[84] G. Porod, General theory, in: Small Angle X-Ray Scattering, Academic Press, New York, 1982, pp. 17–52.

[85] D. Klemm, B. Philipp, T. Heinze, U. Heinze, W. Wagenknecht, Systematics of cellulose functionalization, in: Comprehensive Cellulose Chemistry, Wiley-VCH, Weinheim, 1998, pp. 133–140, doi:10.1002/3527601937.ch1e.

[86] F. Rol, C. Sillard, M. Bardet, J.R. Yarava, L. Emsley, C. Gablin, D. Léonard, N. Belgacem, J. Bras, Cellulose phosphorylation comparison and analysis of phosphorate position on cellulose fibers, Carbohydr. Polym. 229 (2020), doi:10.1016/j.carbpol.2019.115294.

[87] A.C. Nuessle, F.M. Ford, W.P. Hall, A.L. Lippert, Some aspects of the cellulose-phosphate-urea reaction, Text. Res. J. 26 (1956) 32–39, doi:10.1177/004051755602600105.

[88] S. Camarero Espinosa, T. Kuhnt, E.J. Foster, C. Weder, Isolation of thermally stable cellulose nanocrystals by phosphoric acid hydrolysis, Biomacromolecules 14 (2013) 1223–1230, doi:10.1021/bm400219u.

[89] Y. Nishiyama, P. Langan, H. Chanzy, Crystal structure and hydrogen-bonding system in cellulose Iβ from synchrotron X-ray and neutron fiber diffraction, J. Am. Chem. Soc. 124 (2002) 9074–9082, doi:10.1021/ja0257319.

[90] R.H. Colton, D.E. Henn, Crystal structure of disodium orthophosphite pentahydrate, J. Chem. Soc. A Inorg. Phys. Theor. (1971) 1207–1209, doi:10.1039/J19710001207.

[91] P. Kienzle, Neutron activation and scattering calculator, (n.d.). https://www.ncnr.nist.gov/resources/activation/(accessed August 6, 2023).

[92] J.W. Larson, K.G. Zeeb, L.G. Hepler, Heat capacities and volumes of dissociation of phosphoric acid (1st, 2nd, and 3rd), bicarbonate ion, and bisulfate ion in aqueous solution, Can. J. Chem. 60 (1982) 2141–2150, doi:10.1139/v82-306.

[93] Phosphoric Acid-d3 Solution; MSDS 176753, Sigma-Aldrich Co. LLC, St. Louis MO USA, 2022 [Online] https://www.sigmaaldrich.com/US/en/sds/aldrich/176753 accessed June 22, 2022.

[94] E.P. Egan, B.B. Luff, Measurements at 15° to 80°C. - density of aqueous solutions of phosphoric acid, Ind. Eng. Chem. 47 (1955) 1280–1281, doi:10.1021/ie50546a062.

[95] M. Shibayama, Spatial inhomogeneity and dynamic fluctuations of polymer gels, Macromol. Chem. Phys. 199 (1998) 1–30, doi:10.1002/(SICI)1521-3935(19980101)199:1⟨1::AID-MACP1⟩3.0.CO;2-M.

[96] A.J. Hurd, D.W. Schaefer, J.E. Martin, Surface and mass fractals in vapor-phase aggregates, Phys. Rev. A 35 (1987) 2361–2364 (Coll Park), doi:10.1103/PhysRevA.35.2361.

[97] P.W. Schmidt, Small-angle scattering studies of disordered, porous and fractal systems, J. Appl. Crystallogr. 24 (1991) 414–435, doi:10.1107/S0021889891003400.

[98] Y. Talmon, Radiation damage to organic inclusions in ice, Ultramicroscopy 14 (1984) 305–315, doi:10.1016/0304-3991(84)90098-6.

[99] Y. Talmon, The study of nanostructured liquids by cryogenic-temperature electron microscopy–a status report, J. Mol. Liq. 210 (2015) 2–8, doi:10.1016/j.molliq.2015.03.054.

[100] O. Kleinerman, A.N.G. Parra-Vasquez, M.J. Green, N. Behabtu, J. Schmidt, E. Kesselman, C.C. Young, Y. Cohen, M. Pasquali, Y. Talmon, Cryogenic-temperature electron microscopy direct imaging of carbon nanotubes and graphene solutions in superacids, J. Microsc. 259 (2015), doi:10.1111/jmi.12243.

[101] A. Matatyaho Ya'Akobi, Y. Talmon, Extending Cryo-EM to nonaqueous liquid systems, Acc. Chem. Res. 54 (2021) 2100–2109, doi:10.1021/acs.accounts.1c00077.

[102] V.A. Platonov, Properties of polyphosphoric acid, Fibre Chem. 32 (2000) 325–329, doi:10.1023/A:1004199406779.